AIP | Review of Scientific Instruments

Pound-Drever-Hall-locked, frequency-stabilized cavity ring-down spectrometer

A. Cygan, D. Lisak, P. Masłowski, K. Bielska, S. Wójtewicz, J. Domysławska, R. S. Trawiński, R. Ciuryło, H. Abe, and J. T. Hodges

Citation: Review of Scientific Instruments **82**, 063107 (2011); doi: 10.1063/1.3595680
View online: http://dx.doi.org/10.1063/1.3595680
View Table of Contents: http://scitation.aip.org/content/aip/journal/rsi/82/6?ver=pdfcov
Published by the AIP Publishing

Pound-Drever-Hall-locked, frequency-stabilized cavity ring-down spectrometer

A. Cygan,[1] D. Lisak,[1] P. Masłowski,[1,a)] K. Bielska,[1] S. Wójtewicz,[1] J. Domysławska,[1] R. S. Trawiński,[1] R. Ciuryło,[1] H. Abe,[2] and J. T. Hodges[3]
[1]*Instytut Fizyki, Uniwersytet Mikołaja Kopernika, ul. Grudziadzka 5/7, 87-100 Toruń, Poland*
[2]*National Metrology Institute of Japan (NMIJ), AIST, Tsukuba Central 3, Tsukuba 305-8563, Japan*
[3]*National Institute of Standards and Technology, 100 Bureau Drive, Gaithersburg, Maryland 20899, USA*

(Received 30 March 2011; accepted 8 May 2011; published online 16 June 2011)

We describe a high sensitivity and high spectral resolution laser absorption spectrometer based upon the frequency-stabilized cavity ring-down spectroscopy (FS-CRDS) technique. We used the Pound-Drever-Hall (PDH) method to lock the probe laser to the high-finesse ring-down cavity. We show that the concomitant narrowing of the probe laser line width leads to dramatically increased ring-down event acquisition rates (up to 14.3 kHz), improved spectrum signal-to-noise ratios for weak O_2 absorption spectra at $\lambda = 687$ nm and substantial increase in spectrum acquisition rates compared to implementations of FS-CRDS that do not incorporate high-bandwidth locking techniques. The minimum detectable absorption coefficient and the noise-equivalent absorption coefficient for the spectrometer are about 2×10^{-10} cm^{-1} and 7.5×10^{-11} cm^{-1}Hz$^{-1/2}$, respectively. © *2011 American Institute of Physics*. [doi:10.1063/1.3595680]

I. INTRODUCTION

The cavity ring-down spectroscopy (CRDS) technique dates from the seminal work of O'Keefe and Deacon in 1988 (Ref. 1) in which a pulsed laser was used to pump a resonant optical cavity filled with a light-absorbing gas. They showed that the absorption spectrum could be determined by measuring the wavelength dependence of the cavity photon decay time. This and other early realizations of CRDS (Refs. 2–7) used pulsed lasers with bandwidths that exceeded the cavity mode spacing, thereby ensuring spectral overlap between the pump laser and narrow line width cavity resonances. However, the forced overlap of multiple cavity resonances (each having its own characteristic decay time) meant that the spectral resolution was limited by the probe laser bandwidth and also ensured that the cavity decay signals were multi-exponential.[8,9] These complications made it difficult to quantify the effects of laser bandwidth on the ordinate (absorption) and abscissa (frequency) axes of the CRDS absorption spectra.[7,10–12] Also, the wide bandwidth of the pulsed lasers and the relatively low repetition rates (typically 10 Hz or less) employed in early CRDS experiments limited the coupling efficiency, data acquisition rate, and signal-to-noise ratio of the acquired spectra. To overcome these limitations of pulsed CRDS, in the 1990s single-mode continuous wave (cw) lasers were introduced in ring-down experiments[10,13,14] and are now commonly used. The relatively narrow line width of cw lasers enables the selective excitation of individual cavity modes, which leads to single exponential decays and improved decay-time measurement statistics. As discussed by Berden *et al.* in their review,[15] for cw-CRDS techniques relative standard deviations of decay time constant of the order 0.03% have been demonstrated, while for pulsed CRDS experiments they generally exceed 1%. However, the narrow line width excitation afforded by cw lasers requires that the probe laser and local ring-down cavity mode must be actively brought into spectral coincidence. In 1995 Romanini *et al.*[13] first solved this problem in cw-CRDS setups by slow modulation of the cavity optical length, with the mean cavity length actively servoed to maintain coincidence between a local TEM_{00} mode and the probe laser frequency. In order to avoid beats in light decays, the laser beam was interrupted by an acousto-optic modulator (AOM). This cw laser beam switching technique is now widely used in cw-CRDS experiments. The sensitivity of Romanini's cw-CRDS spectrometer was tested on the weak HCCH overtone transitions near $\lambda = 570$ nm for which they obtained a minimum detectable absorption of 10^{-9} cm^{-1}.[14]

Because of its high sensitivity, the CRDS technique is currently regarded as an essential tool for trace gas detection and measurements of weak absorption spectra. It plays an important role in long-path atmospheric observations where, for example, solar spectra reveal relatively weak absorption from electric quadrupole transitions[16] and magnetic dipole transitions in the O_2 *A*-band.[17,18] The long effective optical path lengths achievable with CRDS have made it possible to measure these[19–21] and other low-intensity (as low as 2.5×10^{-31} cm^{-1}/(molecule cm^{-2})) transitions[21,22] in the laboratory using relatively compact sample volumes.

Despite the impressive capabilities demonstrated with CRDS, there are ongoing efforts to lower the detection limit. Martínez *et al.*[23] discussed several ways of increasing CRDS sensitivity, where the most obvious approaches theoretically involve increasing the cavity length or using mirrors with higher reflectivity. The respective drawbacks of these approaches are the practical limitation of making extremely long cavities and the reduced amount of light that can be injected

a)Present address: JILA, National Institute of Standards and Technology and University of Colorado Department of Physics, University of Colorado, Boulder, Colorado 80309-0440, USA.

into the cavity when the mirror reflectivity increases. Ye and Hall[24] demonstrated a near shot-noise-limited absorption sensitivity normalized to a 1-s averaging time of 1.6×10^{-10} using the cavity ring-down heterodyne spectroscopy method. In their experiment, two modes of a ring-down cavity were simultaneously pumped by a pair of phase-coherent, frequency-shifted laser beams. Each beam was periodically interrupted out of phase with the other, thus inducing simultaneous ring-up and ring-down signals. This scheme resulted in a heterodyne beat note between the two probe beams which differentially sampled the absorption line. Importantly, this method involved active locking of the probe laser to the narrow line width (3.5 kHz full-width at half-maximum (FWHM)) cavity resonances using the Pound-Drever-Hall (PDH) method[25] described below.

Presently, the most frequently used approach for increasing the CRDS sensitivity relies on increasing the repetition rate of ring-down events, with the maximum achievable rate being of the order of the reciprocal ring-down time, τ^{-1}. However, the repetition rate in cw-CRDS typically is limited by phase fluctuations in the probe laser and is well below this value. The disparity is a consequence of the relatively narrow resonances (<5 kHz) characteristic of high-finesse ring-down cavities as compared to typical cw laser line widths which range from 0.1 MHz to 5 MHz. This frequency mismatch between the cavity line width and probe laser bandwidth can be overcome by actively locking the probe laser to the cavity resonance. Two techniques have been implemented for this purpose: the PDH method and the self-locking optical feedback (OF) approach. Paldus *et al.*[26] were the first to demonstrate a PDH locking scheme in a cw-CRDS setup. Their experiment incorporated an external cavity diode laser (ECDL) at $\lambda = 833$ nm, an AOM as a rapid light switch and a three-mirror, traveling wave optical resonator in which the *s* and *p* polarizations each had a unique finesse, $\Im$. The resonator was PDH-locked to the ECDL using the lower-finesse *p*-polarization beam ($\Im = 430$), whereas the CRDS decay measurements were made using the higher-finesse *s*-polarization ($\Im = 3300$). Although the empty-cavity ring-down time constants for this setup were relatively short ($\tau = 1$ μs), they achieved a baseline noise of 5×10^{-9} cm^{-1} because their ring-down signals were acquired at a repetition rate of 50 kHz. However, at each laser frequency step within the acquired spectrum the cavity length had to be scanned in order to relock the cavity. Consequently the spectrum frequency axis determination was limited by the wavelength stability of the ECDL. Two years later, there was an improved experiment by the same group[27] which gave a higher ring-down signal repetition rate of 80 kHz and a short-term noise equivalent absorption of 1×10^{-12} cm^{-1}Hz$^{-1/2}$. To this day, this is probably the highest reported sensitivity of any CRDS experiment. The system of unlocking and relocking the laser to the cavity was similar to that of the original paper by Paldus *et al.*[26] so the problem of inaccuracy in the spectrum frequency axis remained unsolved. With regard to the OF approach to CRDS, light from the resonator feeds back to the probe laser thus causing the laser line width to narrow up to that of the ring-down cavity. Morville *et al.*[28] first demonstrated the self-locking OF method on a folded-cavity resonator and obtained a ring-down acquisition rate of 2 kHz and noise-equivalent absorption coefficient equal to 5×10^{-10} cm^{-1}Hz$^{-1/2}$. Comparing the OF and PDH CRDS locking techniques, the former requires a more complicated three-mirror configuration of the cavity than the latter (as given below), whereas the latter needs more advanced electronics for the laser-lock feedback loop.

Fox *et al.*[29] also extensively discussed the combination of cw-CRDS with the PDH laser locking technique. They proposed a new system of unlocking and relocking the probe laser to the cavity, which allows rapid recovery of the lock after measurement of light decay and which does not require a three-mirror, polarization-dependent cavity configuration. This technique was subsequently applied by van Leeuwen *et al.*[30] in 2003. Their minimum detectable absorption loss was only 4.7×10^{-9} cm^{-1} with a 16 kHz decay repetition rate, but as was shown a faster analog-to-digital converter should have provided a value of 5.9×10^{-10} cm^{-1}Hz$^{-1/2}$. Because of the small laser tuning range of $\simeq$4 GHz, calibration of the spectrum frequency axis was difficult for this spectrometer. This problem did not appear in PDH-locked CRDS experiment proposed by Martínez *et al.*[23] in 2006, where the range of the frequency scan was about 30 GHz. They demonstrated the PDH and CRDS method on a two-mirror, high-finesse ($\Im > 15\,000$) ring-down cavity, with the laser locked to the cavity. Compared to PDH-locked cavity ring-down spectrometers discussed above, which were operated over a rather small frequency scanning range, the spectrometer of Martínez *et al.*[23] can be considered to be a more practical spectroscopic tool because it combines high sensitivity and broad tunability. However, the problem of precision and accuracy in the frequency axis, also common to other CRDS setups, was not considered by Martínez *et al.*

The spectrometer built in 2004 by Hodges *et al.* of the National Institute of Standards and Technology (NIST) in Gaithersburg,[31,32] was designed to exploit the inherent frequency-selectivity of high-finesse ring-down cavities (abscissa-axis) in addition to the high-sensitivity in absorption coefficient (ordinate-axis) afforded by single-mode CRDS. This system was the first to provide exceptionally high spectral resolution measurements of weak absorption spectra (e.g., <1 MHz-wide saturation dips) that were limited by the frequency stability of the ring-down cavity rather than the probe laser frequency stability.[33,34] To this end, the cavity modes were actively stabilized with respect to an AOM-tuned, frequency-stabilized reference laser, and the cw-probe laser frequency was locked to individual TEM_{00} cavity modes. Importantly, the servo used to lock the probe laser merely eliminated the laser drift, but did not have enough bandwidth to tighten up the cw-laser line width to match that of the cavity. Nevertheless, this technique decoupled the cavity stabilization from the probe laser frequency jitter and drift. A pair of dichroic mirrors formed the optical cavity. They were double coated in order to yield relatively high and low losses for the reference laser and probe laser, respectively. Stabilization of the cavity length yielded equidistant cavity modes suitable as high-precision frequency markers in spectral scans. In this scheme, the frequency resolution was limited by the stability of reference laser, which was less than about

0.5 MHz. This technique, referred to as frequency-stabilized cavity ring-down spectroscopy (FS-CRDS), has been used to measure line parameters of near-infrared transitions of water vapor and O_2. The relative uncertainties in the line intensities were typically less than 0.5%. Observation of subtle line shape effects like collisional narrowing and pressure shifting demonstrated the applicability of the frequency-stabilized cavity ring-down spectroscopy technique for generating reference-quality spectroscopic data required in atmospheric research.

The first FS-CRDS spectra were obtained by manually tuning the cw-probe laser to the actively stabilized cavity resonances. Improvements of this spectrometer in 2005 (Ref. 32) led to automation of probe laser frequency tuning and actively locking it to chosen cavity modes. The minimum noise-equivalent absorption coefficient of the FS-CRDS spectrometer in 2006 (Ref. 35) was about 1.2×10^{-10} $cm^{-1}Hz^{-1/2}$, while the relative uncertainty of water line intensities evolved in relatively short time from 0.6% (2007) (Ref. 34) to less than 0.4% (2009).[36]

In the remainder of this article we present the first PDH-locked FS-CRDS apparatus, which combines both high sensitivity in absorption coefficient determination and high spectral resolution. This apparatus is a result of recent improvements to our previous FS-CRDS spectrometer, which was essentially identical to that built at NIST and which was used for precise line shape measurements in the O_2 B-band near $\lambda = 687$ nm.[37] In the following we discuss our implementation of the PDH technique, resulting in substantial reduction in the laser line width, increased data acquisition rates and spectrum signal-to-noise ratio. In the first section we present the experimental setup after which we compare the new (with PDH lock) and old (without PDH lock) FS-CRDS measurement procedures. Finally, we discuss the role of the PDH lock in our measurement of subtle line shape effects.

II. POUND-DREVER-HALL LASER LOCKING TECHNIQUE

In this study, we use the PDH method[25] to actively narrow the probe laser line width so that it matches that of the ring-down cavity. The PDH method exploits the extremely sharp frequency dependence near resonance in the phase of the reflected field from a high-finesse Fabry-Pérot (FP) resonator. In the absence of absorption, the net reflectivity $\rho(\nu)$ of an incident field of amplitude $E_{\text{inc}} = E_0 e^{i2\pi\nu t}$ and frequency ν is given by

$$\rho(\nu) = \frac{r[e^{i2\pi\delta_\nu/\nu_f} - 1]}{1 - r^2 e^{i2\pi\delta_\nu/\nu_f}}, \tag{1}$$

where r is the amplitude reflection coefficient of the FP mirrors, ν_f is the FP cavity free spectral range, and δ_ν is the frequency difference (detuning) between the incident beam and the local cavity resonance. The light reflected from a FP cavity can be decomposed into two components: the part of the incident field which reflects directly off the input mirror without entering the cavity, and the part of the field circulating within the cavity which leaks out the input mirror back toward the source. On resonance, these two field components are exactly out of phase and of equal magnitude, such that the net reflection from the FP cavity is zero. Importantly, the phase of the reflected field changes sign with that of the detuning, δ_ν. Thus the phase provides directional information that can be used to determine the sign of the error signal. Because photo-detectors are not fast enough to measure directly optical frequencies, the phase of the reflected beam must be determined via a beat note. To this end, in the PDH method the incident beam is typically phase-modulated with a modulation frequency Ω that greatly exceeds the FP cavity line width. Treating the modulated incident beam as a carrier wave at frequency ν of amplitude E_c, with two symmetrically located sidebands at $\nu \pm \Omega$ of amplitude E_s gives the total reflected field as

$$E_r = -E_s\rho(\nu - \Omega) + E_c\rho(\nu) + E_s\rho(\nu + \Omega). \tag{2}$$

Given that the intensity I of the reflected field scales with $|E_r|^2$, it can be shown that for large modulation frequencies, the dominant AC term occurs at Ω and is given by

$$I(\Omega) = 2E_sE_c\text{Im}[\rho(\nu)\rho^*(\nu + \Omega) - \rho^*(\nu)\rho(\nu - \Omega)] \times \sin(2\pi\Omega t), \tag{3}$$

where we have neglected harmonics of Ω. The preceding expression for $I(\Omega)$ represents the anti-symmetric error signal that is used in the PDH technique to correct for frequency mismatch between the probe laser and FP resonator. It can be readily measured by phase modulating the probe beam and monitoring the component of the net reflected signal at the modulation frequency. For small δ_ν, this signal acts as an acutely sensitive frequency discriminator. We evaluated the error signal given by Eq. (3) assuming mirror reflectivities and modulation rates that are similar to those considered in the present experiment. The calculations shown in Fig. 1. illustrate the extremely narrow capture range of the PDH error signal. These calculations also show that for the values of r and Ω considered here, the normalized error signal in Fig. 1. is well approximated by the derivative of the Lorentzian function, $(\Delta\nu_c/2)(1 + 4\delta_\nu^2/\Delta\nu_c^2)^{-1}$, in which $\Delta\nu_c$ is the full width at half maximum (FWHM) of the cavity resonance given by $\nu_f(1 - r^2)/(\pi r)$. More information about the PDH technique can be found in Refs. 25 and 38, where the underlying theory is presented.

III. EXPERIMENTAL SETUP

A. Optomechanical configuration of PDH-locked FS-CRDS setup

A schematic diagram of the PDH-locked FS-CRDS spectrometer, which was built in the Institute of Physics of Nicolaus Copernicus University in Toruń, is presented in Fig. 2. The main part of this spectrometer is the NIST-designed, evacuatable absorption cell,[31] with a nominal length and internal volume equal to 73 cm and 0.2 dm^3, respectively. The resonant optical cavity is created by two concave mirrors, each having a 1 m radius of curvature and diameter of 7.6 mm. The mirrors are arranged in a non-confocal configuration to maximize the separation of low-order transverse modes. One cavity mirror is mounted on a piezo-electric transducer (PZT,

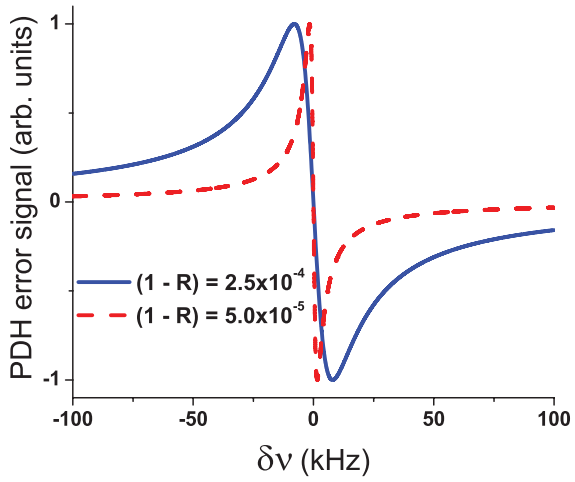

FIG. 1. (Color online) Calculated Pound-Drever-Hall error signals for $\Omega = 20$ MHz, $\nu_f = 200$ MHz, and $R = r^2 = 0.99975$ and 0.99995, respectively based on Eq. (3). Note that $\Delta\nu_c$ (16 kHz and 3 kHz for the respective cases) equals the width of the linear part of the error signal.

Physik Instrumente, Model: S-314.10),[39] which enables control of the mirror-to-mirror distance up to 12 μm in order to compensate for thermal expansion effects. The double-coated mirrors (*Precision Photonics*) have a high reflectivity ($R = 0.99975$) at wavelength $\lambda = 687$ nm, at which our O_2 spectra are measured, and a relatively low reflectivity ($R = 0.98$) at $\lambda = 633$ nm which corresponds to that of the reference HeNe laser used for the cavity length-stabilization servo. To minimize thermal expansion effects, both sides of the cavity are combined by invar rods. The cavity finesse $\Im$, the FWHM cavity line width $\Delta\nu_c$, and the free spectral range (FSR) for $\lambda = 687$ nm are about 12 000, 17 kHz, and 204 MHz, respectively.

The probe laser is a cw, single-mode, ECDL (*Toptica Photonics, Model: DL-Pro*), with a Littrow resonator configuration and temperature and current stabilization. The laser can be coarsely tuned between $\lambda = 684.2$ nm and 692.2 nm via a manually adjustable grating and its mode-hop-free range of operation is about 21 GHz. The laser frequency is measured by a wave meter (WM, *EXFO, Model: WA-1500*) with a combined standard uncertainty of 60 MHz. The single-mode tuning of the ECDL is monitored by a scanning Fabry-Pérot interferometer (FPI, *Toptica Photonics, Model: FPI-110*) with a FSR = 1 GHz. Although the maximum diode laser power is about 20 mW, the amount of light incident on the cavity is about one third as much because of the losses caused by the numerous optical elements along the incident beam path. Because of the narrow free-running line width (≈200 kHz) of the laser, its frequency can be precisely tuned to consecutive cavity modes. An electro-optical modulator (EOM, *Photonics Technologies, Model: EOM-1-20*) shown in Fig. 2 and a fast electronic system for laser frequency control (*Toptica Photonics, Model: FALC 110*) with a bandwidth of 10 MHz are used in order to lock the probe laser to the cavity by the PDH technique. The set of mode matching lenses denoted in Fig. 2. as ML_p and ML_r is used to match the probe and reference laser beam to the TEM_{00} mode of the ring-down cavity. The excited transverse mode of the cavity can be observed by a camera (Cam).

Generation of ring-down events is realized by rapidly switching off the laser beam by an AOM (AOM1, *Brimrose,*

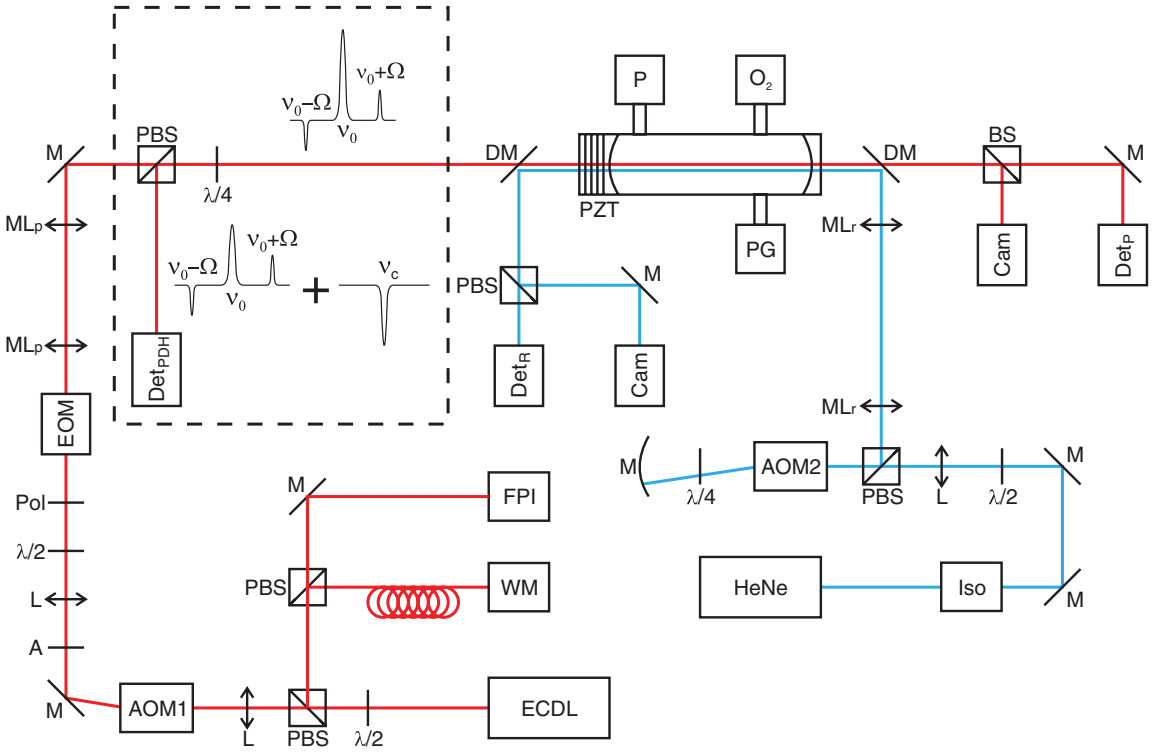

FIG. 2. (Color online) Scheme of optomechanics in PDH-locked FS-CRDS setup. The dashed-line sections indicate the optical signal used by the PDH lock of the probe laser to the ring-down cavity. For clarity, not all optical elements are shown.

Model: TEM-200-50-690). The laser frequency shift caused by AOM1 is nominally 220 MHz. We measured the switching time of AOM1 to be about 50 ns. Light decays are measured by a 10 MHz-bandwidth Si-PIN detector (Det_P, *New Focus, Model: 2051*), and 3000 decays are measured at each frequency step of the measured spectrum. Typical ring-down time constant for the empty cavity is $\approx$9.7 μs. In order to acquire an absorption spectrum, the probe laser frequency is tuned and locked to successive TEM_{00} longitudinal modes. Prior to engaging the high-bandwidth PDH lock at each frequency step, it is necessary to implement a low-bandwidth lock of the laser to the local TEM_{00} mode. This step removes the drift in the laser frequency and ensures that the laser frequency is within the usable capture range of the PDH error signal. The ring-down cavity is actively locked to a frequency-stabilized HeNe laser (*Melles Griot, Model: 25-STP-912-230*), with a long-time frequency stability below 2 MHz (8 h time scale). The typical spectrum frequency interval is equal to one FSR, which is obtained at fixed HeNe frequency. In order to take smaller frequency steps, the HeNe frequency can be shifted using the second AOM (AOM2 *Brimrose, Model: TEF-375-250-633*). The AOM2 operates in frequency range of 300–400 MHz which is multiplied by factor 2 in the double-pass configuration.[31] As a consequence of the cavity length stabilization servo, shifting the HeNe laser frequency in turn shifts the cavity resonances so that the spectrum sampling density is limited only by the stability of the reference laser.

The PDH-locked FS-CRD spectrometer was built in order to investigate spectral line shapes of O_2 for both self- and foreign-broadening cases. Here we consider self-broadening, and we use O_2 (99.999% purity, *Linde Gas*) as the sample gas. All surfaces being in contact with the sample are made of electro-polished stainless steel. Prior to introducing the O_2, the cell is evacuated with a turbo-molecular vacuum pump (P). The gas pressure is measured by a calibrated, temperature-stabilized capacitance-diaphragm gauge (PG, *MKS Baratron, Model: 670*) with a relative uncertainty of 0.05%. Gas pressure is recorded throughout the spectral scan to track variations arising from drift in the cell temperature. The ring-down cavity wall temperature is measured with a Hg thermometer which has a standard uncertainty of 0.1 K.

B. Active stabilization of ring-down cavity length

A detailed description of the cavity length-stabilization servo can be found in Hodges *et al.*[31]. Here we will only describe a brief overview of this technique.

The cavity length stabilization technique uses the transmission of a frequency-stabilized source (i.e., HeNe laser) to enable measurement of the mirror-to-mirror displacement, and a PZT-driven ring-down cavity mirror for external control of the cavity length. Unlike the case for the probe laser, the line width of the reference laser ($\lambda = 633$ nm) is significantly less than the cavity line width (3 MHz) at the same wavelength. Thus, transmission of the reference laser through the ring-down cavity provides a sensitive measure of detuning with respect to a local cavity resonance. Small detunings of the cavity length around the resonance condition yield a time-dependent signal that can be transformed into an error signal for closed loop control of the cavity length. Specifically, the 1-f component of the HeNe transmission is proportional to the magnitude and direction of the frequency detuning error. This error signal is obtained by 1-f demodulation (using phase sensitive detection) of the HeNe beam transmission signal.

The HeNe laser frequency is modulated by AOM2 at a repetition rate of 100 kHz (1-f signal frequency) and modulation depth of 5 MHz. We take the first-order diffracted beam and retro-reflect it through AOM2. Unlike a single-pass through AOM2, the twice-diffracted beam (which is frequency shifted by two times the driving frequency of AOM2) has a constant pointing direction. Optical components for this scheme also include a focusing lens (L), a polarizing beamsplitter (PBS), a quarter wave plate ($\lambda/4$) and spherical mirror used as a retro-reflector. This last element is placed at a distance equal to its radius of curvature from the AOM2. We use a digital lock-in amplifier (*EG&G Instruments, Model: 7260*) for phase-sensitive detection of the transmitted HeNe laser light. The 1-f signal from the lock-in amplifier is input to a proportional-integral (PI) regulator (*Precision Photonics, Model: LB1005*). Both proportional and integral signals are fed back, through a 100 Hz low-pass filter to actuate the PZT, thus closing the servo loop and enabling cavity length stabilization with respect to the reference laser frequency. The latter element suppresses the fastest frequencies in the error signal so that only slow thermally induced changes in the cavity length are compensated. As a result the entire comb of cavity resonance frequencies is stabilized to within the stability of the HeNe laser ($\approx$1 MHz), which corresponds to an absolute mirror-to-mirror length stability of 1.6 nm.

C. PDH technique of laser locking to the high finesse cavity

In this and most cw-CRDS experiments, the mismatch between the free-running probe laser line width (>100 kHz) and the cavity line width (17 kHz) limits the efficiency with which light can be coupled into the ring-down cavity. Even with perfect mode matching, the peak intensity and repetition rate of the ring-down signal will be well below their respective optimal values, thus compromising the measurement statistics for the ring-down time constant τ. When the line widths of the probe laser and cavity are optimally matched, the maximum transmitted peak power equals the incident power, and the maximum ring-down decay repetition rate is of the order $1/(8\tau)$, where the factor of 8 allows for a minimum time period corresponding to 6 ring-down and 2 ring-up time constants.

The PDH setup (see Fig. 2) uses EOM to phase modulate the transmitted light. The amplitude of the EOM modulation is chosen so that only a pair of anti-phase sidebands are generated at $\Omega = \pm 20$ MHz about the optical carrier frequency ν_0 (see Fig. 2 for details) with a sideband-to-carrier intensity ratio of about 1:10. A horizontally polarized probe laser beam passes through the EOM, a polarizing beamsplitter (PBS), and a quarter wave plate (QWP) before being directed into the ring-down cavity. The radiation reflected from the front

cavity mirror consists of light from the two sidebands (which are totally reflected from the cavity) and a fraction of the incident light at the optical carrier frequency. This radiation propagates back through the QWP. Because this light makes two passes through the QWP, the returning beam becomes vertically polarized and is separated from the incident beam by the PBS. It should be noted that the near total reflection of the sidebands from the cavity under conditions when the cavity resonance frequency and carrier frequency are close occurs because Ω is large compared to the width of the cavity resonance. The reflected and redirected light is measured with a 125 MHz bandwidth Si-PIN photoreceiver (*New Focus, Model: 1801*) denoted in Fig. 2. as $\mathrm{Det_{PDH}}$. To measure the beat note amplitude and phase, the AC component of the reflected signal measured by $\mathrm{Det_{PDH}}$ is mixed with the 20 MHz EOM modulation signal. The frequencies of Ω and 2Ω present in the output signal from the mixer are removed by a pair of notch filters.[29] The error signal is used in a high-bandwidth feedback loop to lock the probe laser to the frequency stabilized ring-down cavity. The measured bandwidth of feedback loop has been found about 1 MHz, estimated from the spectral analysis of the PDH error signal. The transmission signal of the probe laser light through the ring-down cavity and corresponding open-loop error signal, recorded by 2 GHz oscilloscope, are shown as function of the laser detuning in Fig. 3. It can be clearly seen from Fig. 4, that the PDH lock caused a four-fold increase in the maximum probe laser beam intensity transmitted through the ring-down cavity.

An important problem encountered when implementing the PDH technique, and which we observed, is associated with a drifting baseline in the error signal. This effect is caused by drift in the angle between the direction of light polarization at the input of the EOM and the direction of its crystal axis. We speculate that this drift is caused by changes in the EOM temperature. This variation in temperature leads to unwanted amplitude modulation of the probe laser light which has passed through the EOM and a polarization-sensitive element. As a result, an additional frequency component (denoted by ν_{add} and equal to Ω) with variable amplitude and phase occurs in the signal recorded by the $\mathrm{Det_{PDH}}$ detector. Because the signal at ν_{add} is always present in the detected signal independently of the optical frequency of the probe laser, its demodulation gives an error signal with a small offset that drifts in time.[29] Consequently, the frequency of the PDH-locked probe laser slowly drifts in time, since the point of locking the laser to the cavity is always zero-crossing of the error signal. This drift in the PDH-locked probe laser frequency leads to inefficiency and eventually leads to problems with relocking the laser to the cavity after ring-down event. In the present experiment, we minimized this problem by thermally isolating the EOM. This approach enabled us to realize the PDH lock for several hours without loss of stability.

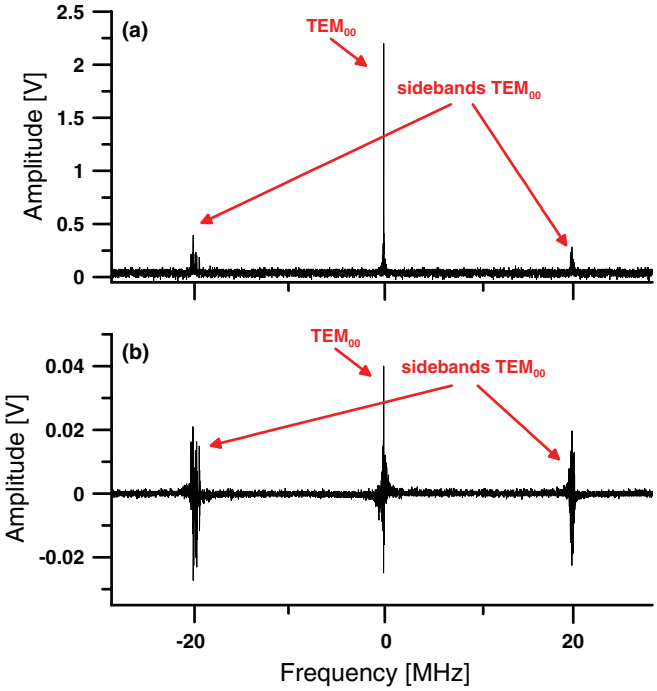

FIG. 3. (Color online) Frequency scan of the probe laser beam through the ring-down cavity recorded by an oscilloscope. (a) Transmission signal through the cavity. (b) Error signal. On both graphs the $\mathrm{TEM_{00}}$ cavity mode and two corresponding sidebands are shown.

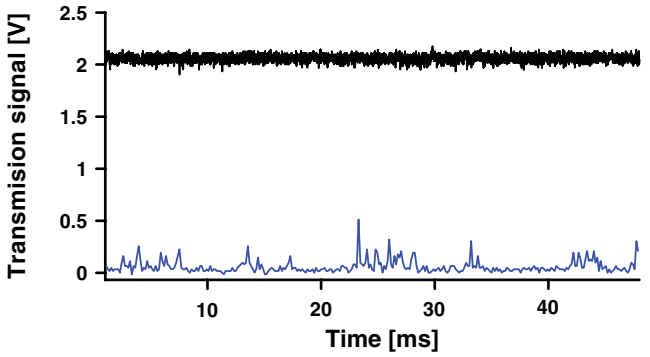

FIG. 4. (Color online) Transmission signal through the cavity recorded with (top, marked black) and without (bottom, marked blue) the PDH lock as a function of time.

In PDH-locked CRDS experiments the acquisition of ring-down decays involves a sequence of three steps: (1) interruption of the probe laser lock, (2) measurement of the decay signal, and (3) laser relocking. In the first ring-down experiments that utilized the PDH technique[26,27] the laser lock to the cavity was completely lost after recording the light decay, and consequently it was necessary to rescan the cavity after each ring-down event for lock recovery. However in the present system, similar to that described in Ref. 24, lock recovery is nearly immediate because of the fast feedback loop and the stability of the locked cavity. The typical acquisition rate of ring-down events generation for our spectrometer is about 14.3 kHz and its upper bound is determined by the ring-down time constant and duration of the acquired ring-down signal, not by the speed at which the laser is relocked.

D. Electronic configuration for the PDH lock

The PDH electrical setup and measurement control electronics are shown in Fig. 5. A 20 MHz RF signal from the PDD block (*Toptica Photonics, Model: PDD 110*) is

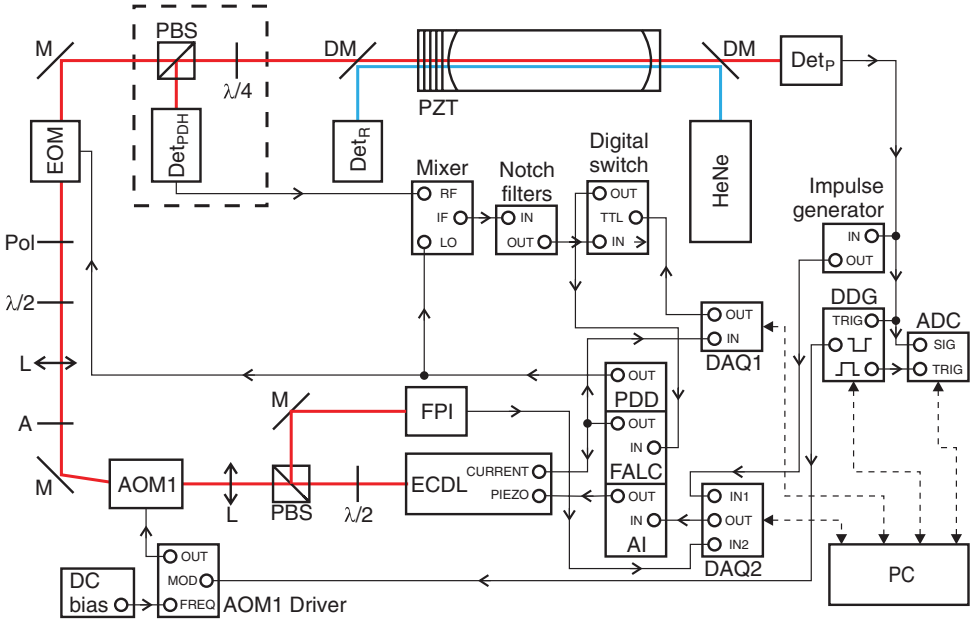

FIG. 5. (Color online) PDH electrical setup and measurement control electronics in the PDH-locked FS-CRD spectrometer. Dashed lines correspond to computer connections. See text for details.

connected to the EOM in order to phase modulate the probe laser beam. This signal also serves as a local oscillator (LO) at the input of the mixer (Mixer, *Mini Circuits, Model: ZP-3-S+*). The AC beat note signal measured by the Det_{PDH} detector is connected to the RF input of the mixer. The FALC PID regulator uses the filtered mixer output as an error signal. Optimization of the FALC parameters enables one to control the probe laser diode current (and hence laser frequency) with a bandwidth greater than 500 kHz. This PID servo enables control of fast fluctuations in the probe laser frequency, thus making the laser line width commensurate with the cavity line width. Slow drifts in the laser frequency caused by temperature and pressure changes are controlled through a LabView program acting as an integrator. The integration rate, which is about 1.4 kHz, is fast enough to keep up with the changing cavity length caused by tuning the HeNe reference laser. The correction voltage from the integrator is added to the voltages set by the DAQ2 card (DAQ2, *National Instruments, Model: PCI-6052E*, 16-bit vertical resolution, 333 kS/s max sampling rate, 480 kHz bandwidth). This error signal is sent through the analog interface (AI, *Toptica Photonics, Model: DCB 110*) to the piezo input of the probe laser head.

The output of the DAQ2 card used by the integrator is also used for automatically tuning the probe laser frequency. Tuning by one FSR of the cavity and relocking to the next cavity TEM_{00} mode requires subdivision of the laser frequency change into 10 equal tuning steps. At each step, a new value of tuning rate dv/dV is determined based on Fabry-Pérot interferometer measurements of the laser tuning. The small corrections of dv/dV are due to the slightly nonlinear dependence of laser frequency on the tuning range. More details about automation of probe laser frequency tuning can be found in Ref. 32.

Ring-down decays are triggered via TTL signals (which are input to the AOM1 RF driver) from a digital delay generator (DDG, *Stanford Research Systems, Model: DG535*). Thus, when the transmitted probe laser signal exceeds a threshold, the probe laser light is switched off to begin a ring-down event. The time delay of the TTL low level is about 55 μs. Decay signals are digitized with an analog-to-digital converter card (ADC, *Gage Applied, Model: Compu Scope 14200*), having a vertical resolution of 14-bits, a maximum sampling rate of 200 MS/s and a bandwidth of 100 MHz. After acquiring an ensemble of ring-down decay signals, the PDH lock is broken and the probe laser frequency is tuned to the next target mode. Prior to the PDH relock, the probe laser is initially locked using a low-bandwidth scheme which compensates for slow frequency drift. Details regarding this locking technique can be found in Hodges *et al.*[32]. To implement this method, we modulate the probe laser frequency at a rate of 5 Hz and depth of 16 MHz. This approach enables us to lock the laser to the target mode by counting transmission pulses which exit the cavity. These measurements (pulse rate vs. detuning) are converted to a histogram having a centroid that is proportional to the error signal. We refer to this locking scheme as the histogram method.

The digital switch indicated in Fig. 5 was used to automatically control the process of PDH locking and unlocking. Depending on the level of the TTL signal supplied from DAQ1 card (DAQ1, *National Instruments, Model: PCI-6070E*, 12-bit vertical resolution, 1.25 MS/s max sampling rate, 1 MHz bandwidth) to the switch, the error signal can be switched on or off. This is required in our experiment because we frequently have to switch back and forth between the PDH lock and low-bandwidth lock. Typically, the PDH lock is only switched on during the measurement of ring-down events and during the tuning of AOM2. Otherwise, the PDH lock is switched off and the probe laser is locked by the low-bandwidth histogram method.

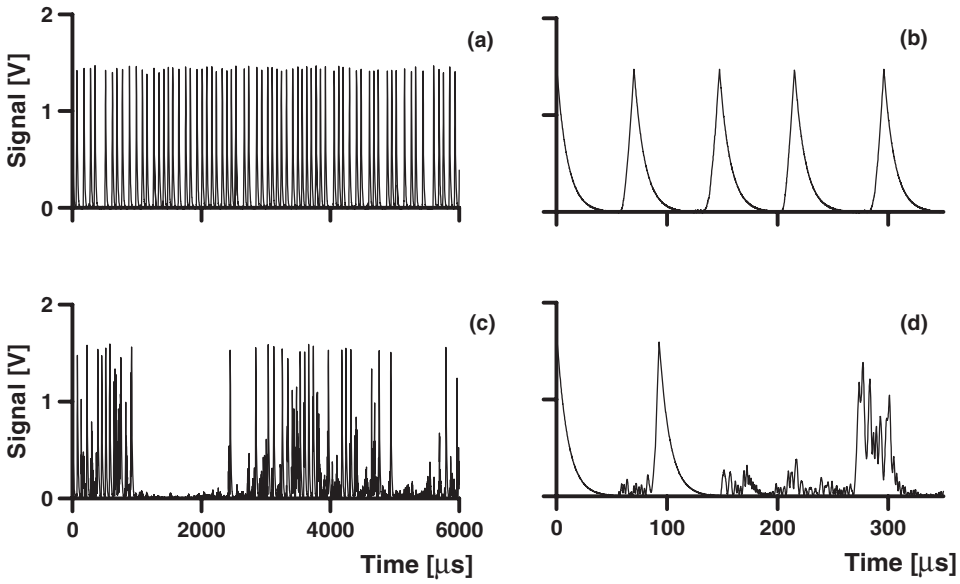

FIG. 6. Ring-down events generation for new PDH-locked FS-CRD (a and b) and histogram-locked FS-CRD (c and d) spectrometers. In the graphs (b) and (d) cavity pumping up and down signals in a short time scale were presented and differences between their shapes can be easily observed. Detector gain in case of (c) and (d) panels is three times higher than for (a) and (b) ones.

IV. INFLUENCE OF PDH LOCK ON PARAMETERS OF PDH-LOCKED FS-CRD SPECTROMETER

Two time series for ring-down decays corresponding to the PDH-locked and histogram-locked FS-CRDS setups, respectively, are presented in Fig. 6. These data, which were all taken at the same DDG threshold level, show dramatically different behavior for the two cases. We note that the detector gain in Figs. 6(c) and 6(d) is three times higher than that of Figs. 6(a) and 6(b), thus indicating that the PDH-lock signals are generally far more intense than the histogram-locked case. Also, it can be easily seen that for the PDH-locked case the ring-down events are periodic in time (graphs (a) and (b)), whereas with the histogram lock, the timing and intensity of the ring-down signals vary randomly in time (graphs (c) and (d)). Without the PDH lock, the timing and intensity of the signals is sensitive to frequency fluctuations in the probe laser. Temporal variations in probe laser frequency which occur on time scales shorter than the intrinsic cavity buildup (or ring-down) time τ, preclude the complete buildup of light intensity in the cavity. Although the histogram locking method eliminates drift in the probe laser, it has insufficient bandwidth to reduce the laser line width, and as a consequence pumping of the cavity exhibits the random fluctuations in timing and intensity shown in Fig. 6(d). With the PDH lock, buildup of the light intensity is limited primarily by τ. The maximum rate at which ring-down events can be obtained depends on the interval between consecutive ring-down events. For the present system, given base losses of $1 - R = 2.5 \times 10^{-4}$, $\tau \approx 9.7\ \mu$s and allowing a total duration of about 1.5τ for the ring-up and 6τ for the ring down signals, gives a period of about $\approx 73\ \mu$s and ring-down signal acquisition rate of 14.3 kHz.

The measurement sensitivity and the optimal number of ring-down signals for averaging can be determined by evaluating the Allan variance[40] of measured τ values. The Allan variance $\sigma_A^2(k)$, is commonly used to characterize spectrometer stability because of its sensitivity to measurement drift. Here we use a simplified form of the Allan variance of a measured quantity X.[41] It is calculated for a series of k equidistant-in-time measurements taken from a full set of N measured values X_n, where $n = 1, ..., N$. It can be given in the form of the following expression

$$\sigma_A^2(k) = \frac{1}{2M} \sum_{m=0}^{M-1} [x_{m+1}(k) - x_m(k)]^2 , \tag{4}$$

where k is the bin size and x_m is a locally averaged value of X. The index k takes on values from 1 to the integer part of $N/2$, and M corresponds to the integer part of $N/k - 1$ which is the upper bound in the series of integers enumerating bins by index $m = 0, ..., M$. Finally, for a given bin width (averaging time),

$$x_m(k) = \frac{1}{k} \sum_{i=1}^{k} X_{m \cdot k + i}, \tag{5}$$

gives the local m-th average of X for the k-element series. The minimum of the Allan variance determines the optimal number of samples k_{opt} that should be averaged to minimize the variance in the mean value of X.

The Allan variance for $k = 1$ ($\sigma_A^2(1)$) is approximately equal to the variance of the series of X_n values. We can use values of $\sigma_A^2(1)$ in order to compare the precision of the two locking techniques based on the single-shot ($k = 1$) uncertainty in τ. Here we take the precision to be proportional to the square root of the Allan variance (Allan deviation), given by $\sigma_A(k)$. Assigning $\sigma_A(k)$ as the Allan deviation of the measured time constants, then $\sigma_A(k)/(c\langle\tau\rangle^2)$ represents the Allan deviation in the loss-per-unit length, where $\langle\tau\rangle$ represents the ensemble mean time constant and c is the speed of light. This quantity is a measure of the minimum detectable absorption coefficient, $\alpha_{\min}(k) = \sigma_A(k)/(c\langle\tau\rangle^2)$ (compared with Refs. 23

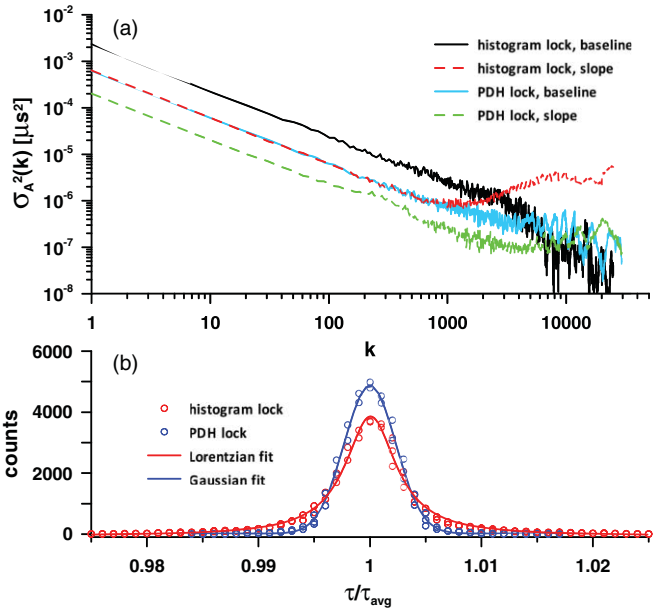

FIG. 7. (Color online) (a) Allan variance of the measured ring-down time constant. Results are given for time series acquired in the baseline and near the maximum slope of the absorption line for the histogram-locked and PDH-locked FS-CRDS spectrometer. (b) Distributions (symbols) of the measured baseline time constants (10 000 point ensembles). The solid lines are a Lorentzian fit and a Guassian fit to the respective distributions. The ring-down signal acquisition rates for the two cases were 25 Hz and 14.3 kHz.

and 30) and was determined for the histogram-locked and PDH-locked cases. We should note that $\alpha_{\min}(1)$ is equivalent to minimum detectable absorption loss in a single shot.[23]

For each of these conditions, τ (and hence $\alpha_{\min}(k)$) was measured in the baseline and with the laser frequency tuned to the maximum slope of the absorption line. These results are given in Fig. 7(a). The values of $\alpha_{\min}(1)$ for the two PDH-locked cases are about half those of the respective histogram-lock cases (see Fig. 7). This improved precision is caused by higher repeatability of the ring-down signal associated with constant light power pumping up the optical cavity in the PDH-locked case (see Figs. 4 and 6). For the histogram-locked case, buildup of intensity in the cavity is relatively noisy because fine frequency fluctuations of the laser are not eliminated by the locking loop. This effect may introduce a small amount of non-exponential behavior in the beginning of the observed decay signals because of the finite extinction rate of AOM1. This would tend to corrupt the ring-down signals and may contribute to additional shot-to-shot variability in the fitted τ. Indeed, there is a clear difference between the shape of the measured distribution of τ values for the two cases (see Fig. 7(b)). The distribution of measured τ values is nearly Gaussian only when the laser is PDH locked to the cavity. For the histogram lock, the distribution has relatively broad wings and resembles a Lorentzian function.

For $k \ll k_{\text{opt}}$, the trend in the Allan deviation reveals that $\alpha_{\min}$ is proportional to $k^{-1/2}$, whereas when $k > k_{\text{opt}}$, additional averaging tends to degrade the measurement precision. We find (see Fig. 7(a)) that k_{opt} is approximately 3000 (nominally 0.2 s) for both sets of PDH-locked measurements. This leads to $\alpha_{\min}(k_{\text{opt}}) \approx 2 \times 10^{-10}$ cm^{-1} estimated for $\sigma_A(3000)/\langle\tau\rangle = 5.1 \times 10^{-5}$ and $\langle\tau\rangle = 9.7$ μs, which is the best-achievable precision in the case of the PDH lock. However, for the histogram-locked case, there is a well defined minimum in the Allan deviation at $k = 1200$ (corresponding to a time scale of approximately 1 min) only for the absorption case; no clear minimum occurs in the baseline-based Allan deviation. This result suggests that for the histogram-lock, drift in the sample conditions or in the frequency axis may be the primary instability. In the case of the high-repetition rate PDH lock, the relatively short time scale for optimal averaging likely has a different origin.

Another commonly used figure of merit for spectrometers is the noise-equivalent absorption coefficient (NEA), which we define as $\alpha_{\min}(1) f_{\text{rep}}^{-1/2}$ (see, e.g., Refs. 23 and 30), where f_{rep} is the ring-down signal repetition rate. Using our measured value of $f_{\text{rep}} = 14.3$ kHz for the PDH-locked setup a NEA equal to 7.5×10^{-11} cm^{-1}Hz$^{-1/2}$ with $\sigma_A(1)/\langle\tau\rangle = 2.6 \times 10^{-3}$ is obtained. By comparison we obtained a NEA of 3.5×10^{-9} cm^{-1}Hz$^{-1/2}$ with $\sigma_A(1)/\langle\tau\rangle = 5.0 \times 10^{-3}$ and $f_{\text{rep}} = 25$ Hz for the histogram-locked measurements. This comparison illustrates the large benefits in measurement statistics that are provided by the high-bandwidth PDH lock. Comparing NEA coefficients determined here with those from other authors it is necessary to pay attention on factor of $\sqrt{2}$ which can appear in some NEA definitions.

V. COMPARISON OF MEASUREMENT PROCEDURES

Comparison of measurement procedures will be made for typical experimental conditions. In case of histogram method the number of acquired ring-down decays was typically limited to 300 to keep relatively short time of measurements. On the other hand for PDH-locked method we can easily operate in the optimal conditions using 3000 decays.

The high ring-down decay repetition rate that was achieved with the PDH-lock required that we alter our measurement and data acquisition procedures. In Fig. 8 we compare the old (histogram-lock case) and new (PDH-lock case) measurement procedures. In both cases we begin by initializing all measurement parameters (steps A and 1 in Fig. 8). This step includes setting the number of AOM2 tuning points (m) and the number of probe laser frequency jumps (N) between adjacent cavity modes. In step B of the old procedure the low-bandwidth lock of the probe laser to the cavity is engaged while AOM2 is frequency tuned to shift the cavity resonances. Step C involves the acquisition of 300 individual ring-down decays, transfer to memory and fitting and averaging of the ensemble of measured decay times. Steps B and C are repeated m times, followed by the jumping of the probe laser frequency to the next TEM_{00} mode of the cavity (step D). Steps B, C, and D are repeated N times during a spectrum acquisition. With this set of steps, a 6 GHz-wide spectrum of single absorption line can be recorded in about 50 min with 50 MHz point spacing for $N = 30$ and $m = 4$, and in about 11 min without cavity length tuning (FSR point spacing for $N = 30$ and $m = 1$).

In the new measurement procedure (Fig. 8(b)), the high acquisition rates demand that the tuning or jumping and data

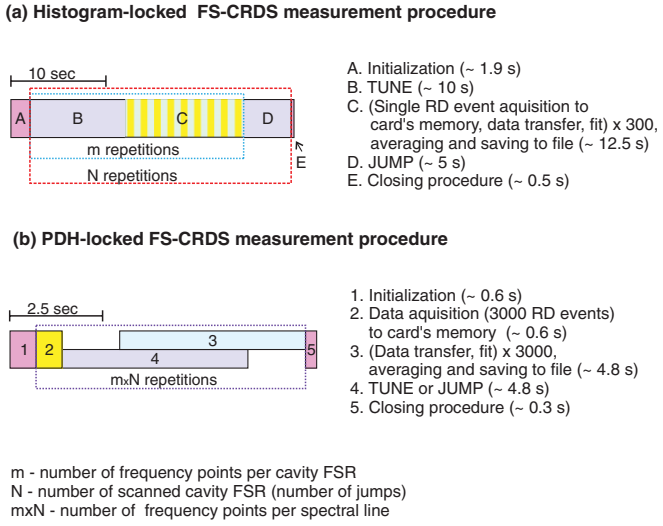

FIG. 8. (Color online) Comparison of measurement procedures for the histogram-locked FS-CRDS and PDH-locked FS-CRDS setups. Typical time periods of each step are presented. See text for more details.

manipulation processes be done in parallel. Thus, in step 2 and beginning with the laser locked to a cavity mode, 3000 light decays are acquired and stored in the memory of the ADC. Subsequently, either tuning or jumping is initiated (step 4) and during realization of either of these processes, data transfer from the ADC to computer memory begins (step 3). Similar to the old procedure, the ring-down decays are fitted individually and the averaged value of the decay time constant is saved to a file (step 3). The delay between steps 3 and 4 is caused by communication between computer cards. As with the old procedure (Fig. 8(a)), for the new procedure (Fig. 8(b)) there are a total of $m \times N$ spectrum measurement points. However, the time to record a 6 GHz-wide absorption line (3000-shot average per spectrum point) with the new procedure is reduced by approximately 4 times, compared to the old procedure (300-shot average), for the same N and m numbers. In order to increase the speed of the cavity tuning between steps 2 and 4, the DDG triggering (see Fig. 5) is switched off. In this way the probe laser lock is not interrupted, making it more resistant to rapid changes in the cavity length. As a result, the speed of the AOM2 tuning is almost 13 times higher than that achieved with the old procedure. This explains why the time period for step 4 is dominated by the time for the probe laser to jump between cavity modes, as is the case for the old measurement procedure in step D.

VI. IMPROVEMENT OF LINE SHAPE MEASUREMENTS

The high spectral resolution and stability of the frequency axis in FS-CRDS enables the investigation of subtle line shape effects. To this end, we evaluated the enhanced performance of our PDH-locked FS-CRDS system by probing a weak transition of the O_2 B-band ($b^1\Sigma_g^+ \leftarrow X^3\Sigma_g^-$, $(\nu' = 1) \leftarrow (\nu'' = 0)$). The wave number and intensity of this transition, which are taken from the HITRAN 2008 database,[42] are 14546.008735 cm^{-1} and 5.886×10^{-25} cm^{-1}/(molecule cm^{-2}), respectively. Although we have previ-

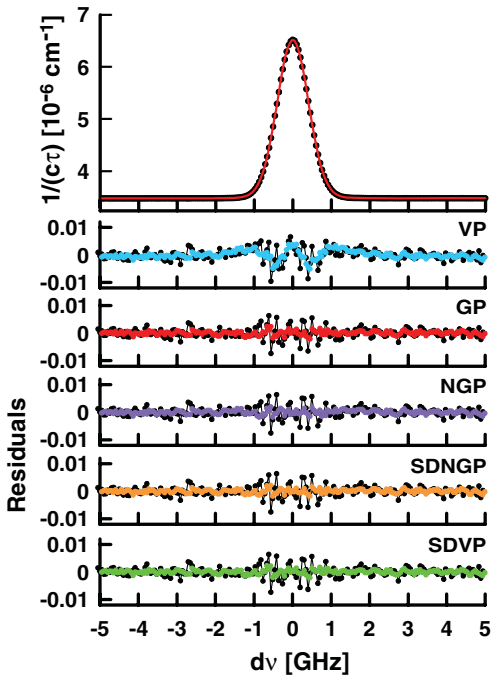

FIG. 9. (Color online) Experimental spectrum of O_2 line at pressure 667 Pa and residuals from fits of different models (VP, GP, NGP, SDNGP, SDVP). Residuals obtained for the histogram-locked FS-CRDS system are these with bigger scatter compared to PDH-locked FS-CRDS system.

ously reported FS-CRDS measurements of this transition,[37] here we quantify how the PDH locking of the probe laser improves the spectrum measurements.

In the top panel of Fig. 9, we present a measured PDH-locked FS-CRDS spectrum (dots) which was taken at a sample pressure of 667 Pa (5 Torr) of pure O_2. The solid line in the top panel represents a least-squares fit of the speed-dependent Nelkin-Ghatak profile (SDNGP) (Refs. 43 and 44) to the measured spectrum. The bottom panels give residuals from fits of several line shape models to the PDH-locked (colored lines) and to the histogram-locked (black lines) FS-CRDS data. Other line profiles that we considered include: Voigt profile (VP), Galatry profile (GP),[45] Nelkin-Ghatak profile (NGP),[43,46] and speed-dependent Voigt profile (SDVP).[47] It can be seen in Fig. 9 that (for a given profile) both sets of residuals have similar shapes, but the random noise is significantly smaller in the data acquired with the PDH lock. The signal-to-noise ratios (SNR, defined here as the ratio of peak absorption to standard deviation of the baseline) in case of GP fits obtained for the histogram-lock and PDH-lock cases are 1600 and 4500, respectively. From the residual plots in Fig. 9, it is clear that the VP (with fixed Doppler width corresponding to the gas temperature and O_2 mass) fails to properly model the measured spectrum. This result suggests that line narrowing effects need to be accounted for in order to model the observed line shape. We note that both the GP (soft-collision model) and NGP (hard-collision model) account for Dicke narrowing. The SDVP is a generalization of the VP in which speed-dependent broadening and shifting effects are considered in the absence of Dicke narrowing. The SDNGP is the most general model considered here because it incorporates both Dicke narrowing and speed dependent effects. It

is possible that both speed-dependent effects as well as Dicke narrowing play important roles in this case. In order to properly analyze the line shape effect, a set of line profiles should be measured over a broad pressure range and analyzed simultaneously using a multi-spectrum fit procedure,[48] see also Refs. 37, 49, and 50. We expect that our improved FS-CRDS setup will be an ideal tool for this type of analysis.

VII. CONCLUSIONS

The PDH-locked spectrometer presented in this paper involves recent improvements to our previously reported FS-CRDS system.[37] The high-bandwidth PDH lock of the probe laser to the narrow resonances of the ring-down cavity enabled us to achieve ring-down signal acquisition rates up to 14.3 kHz, which represents a 500-fold increase in acquisition rate. This capability also yields signal-to-noise ratios in the decay signal approximately 3 times higher and spectrum acquisition rates 4 times faster than were achieved with our low-bandwidth probe laser lock. A natural application of this technique is to support spectroscopic databases like HITRAN that are critical for remote sensing of the Earth's atmosphere. Some of the most demanding applications, for example satellite- and ground-based absorption measurements due to relatively weak bands of atmospheric CO_2 and O_2, require line parameter reference data at the 0.3% uncertainty level.[51] Further, it is now well established that the most accurate line parameter measurements require line shape models (see Ref. 52 for details) that are more sophisticated than the Voigt profile which is typically used in databases. Moreover, recent interest in an independent spectroscopic determination of the Boltzmann constant in terms of the measured Doppler width[53–55] presents a new application for CRDS methods. Errors associated with extrapolating the Doppler width to zero pressure can be reduced by using a high sensitivity technique such as CRDS. Nevertheless, we note that this approach may not be sufficient to avoid systematic relative uncertainties at the 10^{-6} level, and consequently more detailed knowledge about line shape variation over a much wider range of conditions may be required.[56] We believe that our new spectrometer is a promising tool for these and other investigations that require high spectral resolution and high sensitivity.

ACKNOWLEDGMENTS

The authors would like to thank Dr. Tetsuya Ido for valuable discussions about PDH lock technique. The research is part of the program of the National Laboratory FAMO in Toruń, Poland and supported by the Polish MNISW Projects Nos. N N202 1255 35 and N N202 1489 33. Joseph T. Hodges also acknowledges the support of the NIST Greenhouse Gas Measurements Program.

[1] A. O'Keefe, D. A. G. Deacon, Rev. Sci. Instrum. **59**, 2544 (1988).
[2] A. O'Keefe, J. J. Scherer, A. L. Cooksy, R. Sheeks, J. Heath, and R. J. Saykally, Chem. Phys. Lett. **172**, 214 (1990).
[3] D. Romanini and K. K. Lehmann, J. Chem. Phys. **99**, 6287 (1993).
[4] T. Yu and M. C. Lin, J. Am. Chem. Soc. **115**, 4371 (1993).
[5] D. Romanini and K. K. Lehmann, J. Chem. Phys. **102**, 633 (1995).
[6] J. J. Scherer, D. Voelkel, D. J. Rakestraw, J. B. Paul, C. P. Collier, R. J. Saykally, and A. O'Keefe, Chem. Phys. Lett. **245**, 273 (1995).
[7] R. T. Jongma, M. G. H. Boogaarts, I. Holleman, and G. Meijer, Rev. Sci. Instrum. **66**, 2821 (1995).
[8] K. K. Lehmann and D. Romanini, J. Chem. Phys. **105**, 10263 (1996).
[9] J. T. Hodges, J. P. Looney, and R. D. van Zee, J. Chem. Phys. **105**, 10278 (1996).
[10] G. Meijer, M. G. H. Boogaarts, R. T. Jongma, D. H. Parker, and A. M. Wodtke, Chem. Phys. Lett. **217**, 112 (1994).
[11] P. Zalicki and R. N. Zare, J. Chem. Phys. **102**, 2708 (1995).
[12] J. T. Hodges, J. P. Looney, and R. D. van Zee, Appl. Opt. **35**, 4112 (1996).
[13] D. Romanini, J. Gambogi, and K. K. Lehmann, in *50th International Symposium on Molecular Spectroscopy*, edited by T. A. Miller (ACS, Ohio State University, Columbus, OH, 1995).
[14] D. Romanini, A. A. Kachanov, N. Sadeghi, and F. Stoeckel, Chem. Phys. Let. **264**, 316 (1997).
[15] G. Berden, R. Peeters, and G. Meijer, Int. Rev. Phys. Chem. **19**, 565 (2000).
[16] J. W. Brault, J. Mol. Spectrosc. **80**, 384 (1980).
[17] B. van Diedenhoven, O. P. Hasekamp, and I. Aben, Atmos. Chem. Phys. **5**, 2109 (2005).
[18] N. Fournier, P. Stammes, M. de Graaf, R. van der A, A. Piters, M. Grzegorski, and A. Kokhanovsky, Atmos. Chem. Phys. **6**, 163 (2006).
[19] H. Naus, A. de Lange, and W. Ubachs, Phys. Rev. A **56**, 4755 (1997).
[20] D. A. Long, D. K. Havey, M. Okumura, H. M. Pickett, C. E. Miller, and J. T. Hodges, Phys. Rev. A **80**, 042513 (2009).
[21] D. A. Long, D. K. Havey, M. Okumura, C. E. Miller, and J. T. Hodges, J. Quant. Spectrosc. Radiat. Transf. **111**, 2021 (2010).
[22] O. Leshchishina, S. Kassi, I. E. Gordon, L. S. Rothman, L. Wang, and A. Campargue, J. Quant. Spectrosc. Radiat. Transf. **111**, 2236 (2010).
[23] R. Z. Martínez, M. Metsälä, O. Vaittinen, T. Lantta, and L. Halonen, J. Opt. Soc. Am. B **23**, 727 (2006).
[24] J. Ye and J. L. Hall, Phys. Rev. A **61**, 061802 (2000).
[25] R. W.P. Drever, J. L. Hall, F. V. Kowalski, J. Hough, G. M. Ford, A. J. Munley, and H. Ward, Appl. Phys. B **31**, 97 (1983).
[26] B. A. Paldus, C. C. Harb, T. G. Spence, B. Wilke, J. Xie, J. S. Harris, and R. N. Zare, J. Appl. Phys. **83**, 3991 (1998).
[27] T. G. Spence, C. C. Harb, B. A. Paldus, R. N. Zare, B. Willke, and R. L. Byer, Rev. Sci. Instrum. **71**, 347 (2000).
[28] J. Morville, S. Kassi, M. Chenevier, and D. Romanini, Appl. Phys. B **80**, 1027 (2005).
[29] R. W. Fox, C. W. Oates, and L. W. Hollberg, "Stabilizing diode lasers to high-finesse cavities," in *Cavity-Enhanced Spectroscopies*, edited by R. D. Van Zee and J. P. Looney (Academic Press, New York, 2002).
[30] N. J. van Leeuwen, J. C. Diettrich, and A. C. Wilson, Appl. Opt. **42**, 3670 (2003).
[31] J. T. Hodges, H. P. Layer, W. M. Miller, and G. E. Scace, Rev. Sci. Instr. **75**, 849 (2004).
[32] J. T. Hodges and R. Ciuryło, Rev. Sci. Instrum. **76**, 023112 (2005).
[33] D. Lisak, J. T. Hodges, and R. Ciuryło, Phys. Rev. A **73**, 012507 (2006).
[34] D. Lisak and J. T. Hodges, Appl. Phys. B **88**, 317 (2007).
[35] J. T. Hodges and D. Lisak, Appl. Phys. B **85**, 375 (2006).
[36] D. Lisak, D. K. Havey, and J. T. Hodges, Phys. Rev. A **79**, 052507 (2009).
[37] D. Lisak, P. Masłowski, A. Cygan, K. Bielska, S. Wójtewicz, M. Piwiński, J. T. Hodges, R. S. Trawiński, and R. Ciuryło, Phys. Rev. A **81**, 042504 (2010).
[38] E. D. Black, Am. J. Phys. **69**, 79 (2000).
[39] Commercial equipment, instruments, materials, or software are identified in this report to specify adequately the experimental procedure. Such identification does not imply recommendation or endorsement of these items by NIST, nor does it imply that they are the best available for the purpose.
[40] D. W. Allan, Proc. IEEE **54**, 221 (1966).
[41] P. W. Werle, K. Josek, and F. Slemr, Proc. SPIE **1433**, 128 (1991).
[42] L. S. Rothman, I. E. Gordon, A. Barbe, D. Chris Benner, P. F. Bernath, M. Birk, V. Boudon, L. R. Brown, A. Campargue, J.-P. Champion, K. Chance, L. H. Coudert, V. Dana, V. M. Devi, S. Fally, J.-M. Flaud, R. R. Gamache, A. Goldman, D. Jacquemart, I. Kleiner, N. Lacome, W. J. Lafferty, J.-Y. Mandin, S. T. Massie, S. N. Mikhailenko, C. E. Miller, N. Moazzen-Ahmadi, O. V. Naumenko, A. V. Nikitin, J. Orphal, V. I. Perevalov, A. Perrin, A. Predoi-Cross, C. P. Rinsland, M. Rotger, M. Šimečková, M. A. H. Smith, K. Sung, S. A. Tashkun, J. Tennyson, R. A. Toth, A. C. Vandaele, and J. Vander Auwera, J. Quant. Spectrosc. Radiat. Transf. **110**, 533 (2009).

[43]S. G. Rautian and I. I. Sobelman, Usp. Fiz. Nauk **90**, 209 (1966) [Sov. Phys. Usp. **9**, 701 (1967)].
[44]B, Lance, G. Blanquet, J. Walrand, and J. P. Bouanich, J. Molec. Spectrosc. **185**, 262 (1997).
[45]L. Galatry, Phys. Rev. **122**, 1218 (1961).
[46]M. Nelkin and A. Ghatak, Phys. Rev. **135**, A4 (1964).
[47]P. R. Berman, J. Quant. Spectrosc. Radiat. Transf. **12**, 1331 (1972).
[48]D. C. Benner, C. P. Rinsland, V. Malathy Devi, M. A. H. Smith, and D. Atkins, J. Quant. Spectrosc. Radiat. Transf. **53**, 705 (1995).
[49]A. S. Pine and T. Gabard, J. Quant. Spectrosc. Radiat. Transf. **66**, 69 (2000).
[50]A. S. Pine and R. Ciuryło, J. Mol. Spectrosc. **208**, 180 (2001).
[51]C. E. Miller, L. R. Brown, R. A. Toth, D. Chris Benner, and V. Malathy Devi, C. R. Phys. **6**, 876 (2005).
[52]R. Ciuryło, Phys. Rev. A **58**, 1029 (1998).
[53]C. Lemarchand, K. Djerroud, B. Darquié, O. Lopez, A. Amy-Klein, C. Chardonnet, Ch. J. Bordé, S. Briaudeau, and C. Daussy, Int. J. Thermophys. **31**, 1347 (2010).
[54]A. Merlone, F. Moro, A. Castrillo, and L. Gianfrani, Int. J. Thermophys. **31**, 1360 (2010).
[55]K. M.T. Yamada, A. Onae, F.-L. Hong, H. Inaba, and T. Shimizu, C. R. Phys. **10**, 907 (2009).
[56]A. Cygan, D. Lisak, R. S. Trawiński, and R. Ciuryło, Phys. Rev. A **82**, 032515 (2010).